Rayleigh and acoustic gravity waves detection on magnetograms during the Japanese Tsunami, 2011

V. Klausner,[1,2,3] Esfhan A. Kherani,[2] Marcio T. A. H. Muella,[1] Odim

Mendes,[2] Margarete O. Domingues,[2] and Andres R. R. Papa[3,4]

Corresponding author: V. Klausner, Physics and Astronomy Department, Vale do Paraiba

University - UNIVAP 12244-000, São José dos Campos, SP, Brazil. (virginia@univap.br)

[1]Vale do Paraiba University, São José dos

Campos, SP, Brazil

[2]National Institute for Space Research,

São José dos Campos, SP, Brazil.

[3]Department of Geophysics, National

Observatory, Rio de Janeiro, RJ, Brazil.

[4]State University of Rio de Janeiro, Rio

de Janeiro, RJ, Brazil.

Abstract.   The continuous geomagnetic field survey holds an important

potential in future prevention of tsunami damages, and also, it could be used

in tsunami forecast. In this work, we were able to detected for the first time

Rayleigh and ionospheric acoustic gravity wave propagation in the Z-component

of the geomagnetic field due to the Japanese tsunami, 2011 prior to the tsunami

arrival. The geomagnetic measurements were obtained in the epicentral near

and far-field. Also, these waves were detected within minutes to few hours

of the tsunami arrival. For these reasons, these results are very encouraging,

and confirmed that the geomagnetic field monitoring could play an impor-

tant role in the tsunami warning systems, and also, it could provide addi-

tional information in the induced ionospheric wave propagation models due

to tsunamis.

1. Introduction

The monitoring of the geomagnetic field has proved to be an auxiliary tool in the study of tsunami by several authors [*Balasis and Mandea*, 2007; *Manoj et al.*, 2011; *Utada et al.*, 2011; *Klausner et al.*, 2014a]. The response of the ionosphere to tsunamis and the Rayleigh and gravity waves induced by them has been studied broadly over the years [*Occhipinti et al.*, 2006, 2008, 2010, 2013; *Rolland et al.*, 2010, 2011; *Galvan et al.*, 2012], and modeled [*Occhipinti et al.*, 2011; *Kherani et al.*, 2012].

It is well-known that post-seismic acoustic-gravity and Rayleigh waves can be observable close to the epicenter (in the near-field, within 500 km with velocity up to $\cong 3km/s$) due to direct the vertical displacement of the ground induced by the rupture. Indeed, the rupture, as a Dirac function, have a broad spectrum of energy including both, acoustic and gravity waves as presented on the detailed simulational-observational work by *Kherani et al.* [2012] using TEC and magnetic data. In the far-field, tsunamis induce pure gravity waves, and additionally Rayleigh waves induce pure acoustic waves [*Occhipinti et al.*, 2010]. More details could be found in *Occhipinti et al.* [2013].

The theoretical and observational evidences show that tsunamis can generate Rayleigh and acoustic gravity waves (AGWs) in the atmosphere/ionosphere by tsunami-atmosphere-ionosphere (TAI) dynamic coupling, and this coupling effect do not modify the main frequencies of these waves. The presence of varieties of wavefronts propagating with velocity ranging between Rayleigh to AGW velocity was observed and discussed here for the first time using ground magnetic data for the Japanese tsunami, 2011 in the near and far-field (distances above 500 km). These observations reaffirmed the idea that the

magnetogram data can be used as a possible tool for tsunami warnings as it was already discussed by *Klausner et al.* [2014a].

2. Dataset

On the 11th of March at 05 : 46 UT, 2011, a powerful earthquake of magnitude 8.9 M_w generated a catastrophic tsunami which propagated in the Pacific Ocean. The epicenter was centered at 38.3 °N and Long. 142.4 °E, near to the coast of Japan. To study this event, we used the minutely magnetogram data from the Z-component from 9 ground magnetic stations which are displayed on Table 1.

3. Methodology

In the work of *Klausner et al.* [2014a], the wavelet analysis was proofed to be an alternative tool in detection of magnetic fields induced by the tsunami propagation. Nowadays, the discrete wavelet transform (DWT) has been used in many different works in geophysics [*Domingues et al.*, 2005; *Mendes et al.*, 2005; *Mendes da Costa et al.*, 2011; *Klausner et al.*, 2014a, b]. The DWT is based on the multi-scale analysis and local regularities of the signal. Considering ψ as the analyzing wavelet, the wavelet coefficients of these transforms are dependent of two parameters: the scale a and the central position of the wavelet analyzing function translation b.

Here, the orthogonal discrete wavelet transform was used [*Daubechies*, 1992]. The key aspect of this transform is that the amplitude of the wavelet coefficients can be associated to the local polynomial approximation error which can be defined by the choose of the analyzing wavelet.

Using the squared modulus of the wavelet coefficients $|d_k^j|^2$, we can reproduce the discrete scalogram related to a discrete scale and a position, where the scale is related to a dyadic decomposition in levels j, as $a = 2^j$ and the translation is related to discrete position $b = 2^{-j}k$ at level j with $k \in \mathbb{Z}$.

In this context, we have that a signal $f(t)$ can be represented by the expansion

$$f(t) = \sum_{j=-\infty}^{\infty} \sum_{k=-\infty}^{\infty} d_k^j \psi_k^j (2^j t - k), \tag{1}$$

where d_k^j are the wavelet coefficients computed from the L^2 inner-product

$$d_k^j = \int f(t)\, \psi_k^j (2^j t - k)\, dt. \tag{2}$$

The wavelet transform in level $j + 1$ is given by

$$d_k^{j+1} = 2 \sum_m g(m - 2k)\, c_m^j, \tag{3}$$

where g is a high-pass filter, d_k^{j+1} is the wavelet coefficient at level $j + 1$, c_m^j are the scale coefficients at level j, and $m \in \mathbb{Z}$ [see *Domingues et al.*, 2005, more details].

In this work, we use the Daubechies (db2) wavelet function of order 2, and therefore the non-zero low filter values are $h \cong [\frac{1+\sqrt{3}}{4\sqrt{2}}, \frac{3+\sqrt{3}}{4\sqrt{2}}, \frac{3-\sqrt{3}}{4\sqrt{2}}, \frac{1-\sqrt{3}}{4\sqrt{2}}]$. Also, the sampling rate of 1 min, as consequence of the time resolution of the magnetic data, gives the pseudo-periods of the first three levels of $3, 6$ and 12 minutes, [see *Klausner et al.*, 2014b, more details].

4. Results and analysis

Figure 4 displays, on the right side panel, the magnetic observatories geographic distribution, and on the left side panel, the Tsunami Travel Times (TTT) map. In both graphics, the arrows displays the observatories used in three different wave front of the

tsunami propagation direction that we use here to study the tsunamigenic disturbances, and these directions are denoted by the numbers 1, 2 and 3. Also for guiding purposes, we suggest the use of TTT map to determine the approximated tsunami time arrival for each magnetic observatories.

In the sequence, we will present the analysis of each wave front direction case study. The wave front direction number 1 is parallel to the Japanese coast in the west-southwest direction, and in this case the magnetic observatories used are HAR, KAK, TTK and KNY. Figure 1 shows the travel-time diagram (TTD) of a magnetic induced field trends due to the tsunami in the direction 1. As done previous by *Kherani et al.* [2012], the magnetograms of HAR, KAK, TTK and KNY (blue color) have been filtered using a Butterworth filter with 10 to 30 minutes period bandwidth to extract the tsunami-related magnetic induced fields from the external ionospheric activity. Also, the tsunami wave propagation was simulated using the simulation model developed by *Sladen et al.* [2007]; *Sladen and Hérbert* [2008] (black dot-dashed line). The continuous line represents the tsunami wave front propagation with velocity of $\cong 200m/s$, the red dashed line is associated to Rayleigh waves propagation ($\cong 1.3km/s$), and the dashed lines are associated to acoustic gravity waves propagation $\cong 640m/s$. It is well-known that tsunami waves can induce long-wavelength acoustic gravity waves (AGWs) with velocity up to $\cong 800m/s$ and short-wavelength gravity waves with velocity of $\cong 200m/s$ [*Kherani et al.*, 2012], and additionally Rayleigh waves with velocity up to $\cong 2.1km/s$ which can induce pure acoustic waves [*Occhipinti et al.*, 2010]. In Figure 1, Rayleigh and acoustic gravity waves fronts is observed in the presented TTD. It is possible to notice that depending in the distance from the epicenter the acoustic gravity waves can be detected within minutes to hours

before the arrival of the tsunami wave. By this reason, we can discriminate the effect (on the magnetic data) induced by the ionospheric perturbation, from the effect induced by the secondary magnetic field induced directly by the displacement of the oceanic surface (the tsunami).

In Figure 3, panels from bottom (near-field) to top (far-field) correspond to magnetic observatories of HAR, KAK, TTK and KNY, respectively. Each panel, from top to bottom, displays the corresponding magnetogram (Z component), and the square wavelet coefficients for the three first decomposition levels, $(d^j)^2$ for $j = 1, 2, 3$. It is possible to notice that Figure 3 shows an increase of wavelet coefficient amplitudes (WCAs) before of the tsunami arrival which is owing to the contribution from both geomagnetic disturbances and tsunami induced ionospheric disturbances. In particular, following features are evident from Figure 3: (a) The wavelet coefficients are amplified after few minutes of the earthquake, and (b) At TTK and KNY, amplifications are noted few minutes before the tsunami arrival. These features suggest that the observed disturbances in a few minutes after the earthquake may be associated to Rayleigh, and the amplifications few minutes before the tsunami arrival may be associated to the acoustic ionospheric gravity propagation, respectively. However, we can only come to this conclusion if these identified tsunamigenic disturbances are observed also in the TTD. This kind of analysis makes possible to say that these disturbances can be classified to be from seismic and from tsunami origin.

In a near epicentral field (HAR and KAK), the delay between the tsunami and the AGWs is always positive, see *Occhipinti et al.* [2013] for more details. And in the far-field

(TTK and KNY), the AGWs follows the Rayleigh waves arrival, and they can be detected even with 2 hours in advance of the tsunami arrival.

The TTD for the direction 2 is shown in Figure 3 in which the AGWs disturbances are identified following the same strategy as described in the context of Figure 1. The wave front number 2 is towards the open sea waters, and in this case the magnetic observatories used are OTA, CBI and GUA. It can be again said that such identification classifies these disturbances to be associated to AGWs wave propagation ($\cong 700 m/s$) in which appear within a few minutes to hours before the tsunami arrival.

In Figure 5, the vertical component and corresponding three discrete wavelet coefficients for the magnetic observatories of OTA, CBI and GUA as indicated in Figure 4 for the direction 2. We note from Figure 5 that the magnetic disturbances within a few minutes of the earthquake are amplified at all observatories, these amplifications are only due to AGW propagation. In OTA and CBI, the WCAs around $6:00$ UT may or not be associated to the Rayleigh wave propagation. However, these features related to the Rayleigh wave propagation were not detected in the TTD (Figure 3). Also at CBI, the tsunamigenic disturbances after the tsunami arrival are associated to AGW propagation. And these waves have propagation characteristics similar to the tsunami wavefront propagation. For example, the predicted time of the tsunami's arrival by NOAA at Chichijima Island was at $07:14$ UT. The tide gauge measurements registered the tsunami maximum height at $07:46$ UT with amplitudes up to 1.80m. The CBI magnetic observatory shows remarkable wavelet coefficient amplitudes $(d^j)^2 (j = 1, 2, 3)$ due to the tsunami after the tsunami arrival time as well. These increase in WCAs correspond to the AGWs propagation. Also,

Utada et al. [2011] discussed the similarity between the CBI Z-component fluctuations and the IPM fluctuations reported by *Manoj et al.* [2011] due to the AGW point of view.

The TTD for the direction 3 is shown in Figure 5 in which the AGWs disturbances ($\cong 800m/s$) are identified following again the same strategy as mentioned in the context of Figure 1. In this case, the wave front number 3 is parallel to the Japanese coast, and the magnetic observatories used are ESA and MMB. From Figure 7, it can be again said that the magnetic disturbances due to AGWs within a few minutes of the earthquake are amplified at all observatories, while the amplification due to AGWs could be see at MMB in 2 hours in advance of the tsunami arrival. The reason for that is the ESA observatory is near to the epicenter, and an increase of WCA is almost simultaneous to tsunami wave arrival. On the other hand, near to the magnetic observatory of MMB, the initial phase of the tsunami started at $06:38$ UT and reached the maximum height (0.74 m) at $06:57$ UT. The $(d^j)^2 (j = 1, 2, 3)$ showed WCAs around $06:00$ UT which may be due to Rayleigh wave propagation, and again between $07:00$ and $08:00$ UT which might be due to AGW propagation. At $06:57$ UT, when tsunami reached the maximum height, the presence of an increase in the coefficient amplitudes around this time might be due to tsunami maximum height too.

In all the analysis presented above, post-seismic acoustic-gravity and Rayleigh waves were observable close to the epicenter (near-field, within 500 km with velocity up to $\cong 2km/s$) due to direct the vertical displacement of the ground induced by the rupture. Indeed, the rupture, as a Dirac function, have a broad spectrum of energy including both, acoustic and gravity waves. Here, the presence of varieties of wavefronts propagating with velocity ranging between Rayleigh to gravity wave velocity was observed as presented

on the detailed simulational-observational work by *Kherani et al.* [2012] using TEC and magnetic data. However, the Rayleigh wave propagation was only detected here in direction 1, while AGWs were detected in all directions. This assymetry in the distribution of Rayleigh wave propagation was also observed by *Galvan et al.* [2012]; *Kakinami et al.* [2013] in the TEC data. Their studies also found the Rayleigh waves propagating only in the southward direction, although these waves should propagate in all directions.

5. Conclusions

Using filtered magnetograms of the geomagnetic Z-component, and also, the spectral-time diagrams, we presented a detailed TTD with a presence of Rayleigh and AGWs which was not done before for the Japanese tsunami using magnetogram data, 2011. These perturbations presented velocities of 1.3 km/s and 600 − 800 m/s, respectively, with also it is consistent which tsunami-atmosphere-ionosphere coupling theory. These results are in confirmation with the previous studies [*Occhipinti et al.*, 2006, 2008, 2010, 2013; *Rolland et al.*, 2010, 2011; *Galvan et al.*, 2012], however they show new insight into the tsunamigenic magnetic disturbances due to Rayleigh and AGWs on near and far-field distances from the epicenter.

As explained by *Kherani et al.* [2012], the presence of periodicity of order of 8 to 30 minutes in the spectral-time diagrams and, Rayleigh and acoustic gravity waves fronts in the TTDs are the aspects of this work which distinguish the magnetic disturbances of tsunami in the ionosphere from other external magnetic perturbation sources. Also, *Kherani et al.* [2012] have presented the TTD and reported the presence of acoustic disturbances that remained confined to $< 5^o$ which is 500km distance from the epicenter. However, they did not see any acoustic disturbance beyond this distance. In this work,

we presented these disturbances beyond 500 km from the epicenter distance and up to 3 hours of the tsunami arrival.

Also, the fact of Rayleigh waves and AGWs can be detected with a few hours in advance of the tsunami is very encouraging, and shows that the constant monitoring of the geomagnetic field could play an important role to tsunami forecast and tsunami early warning systems.

References

Balasis, G., M. Mandea (2007), Can electromagnetic disturbances related to the recent great earthquakes be detected by satellite magnetometers? *Tectonophysics*, *431*, 173–195.

Daubechies, I. (1992), Ten lectures on wavelets, *In: CBMSNSF Regional Conference Series in Applied Mathematics*, *SIAM*, Philadelphia, PA. Vol. 61.

Domingues, M. O., O. J. Mendes, and A. Mendes da Costa (2005), Wavelet techniques in atmospheric sciences, *Advances in Space Research*, *35*(5), 831–842.

Galvan, D. A., A., Komjathy, M. P., Hickey, P., Stephens, J., Snively, Y. T., Song, M. D., Butala, and A. J., Mannucci (2012), Ionospheric signatures of Tohoku-Oki tsunami of March 11, 2011: Model comparisons near the epicenter. *Radio Science*, *47*(4), RS4003.

Kakinami, Y., M., Kamogawa, S., Watanabe, M., Odaka, T., Mogi, J. Y., Liu, Y. Y., Sun, and T., Yamada (2013) Ionospheric ripples excited by superimposed wave fronts associated with Rayleigh waves in the thermosphere. *Journal of Geophysical Research: Space Physics*, *118*, 905–911.

Kherani, E. A., P. Lognonné, H. Hébert, L. Rolland, E. Astafyeva, G. Occhipinti, P. Coïsson, D. Walwer, E. R. de Paula (2012), Modelling of the total electronic content and magnetic field anomalies generated by the 2011 Tohoku-Oki tsunami and associated acoustic-gravity waves, *Geophysical Journal International*, *191*(3), 1049–1066.

Klausner, V., O., Mendes, M. O., Domingues, A. R. R. Papa, R. H., Tyler, P., Frick, and E. A. Kherani (2014a), Advantage of wavelet technique to highlight the observed geomagnetic perturbations linked to the Chilean tsunami (2010) *Journal of Geophysical Research: Space Physics*, *119*(4), 3077–3093.

Klausner, V., A., Ojeda González, M. O., Domingues, O., Mendes, and A. R. R., Papa (2014b), Study of local regularities in solar wind data and ground magnetograms. *Journal of Atmospheric and Solar-Terrestrial Physics*, *112*(0), 10–19.

Manoj, C., S. Maus, and A. Chulliat (2011), Observation of Magnetic Fields Generated by Tsunamis, *EOS, Transactions American Geophysical Union*, *92*(2), 13–14.

Mendes, O. J., M. O. Domingues, A. Mendes da Costa, and A. L. Clúa de Gonzalez (2005), Wavelet analysis applied to magnetograms: Singularity detections related to geomagnetic storms, *Journal of Atmospheric and Solar-Terrestrial Physics*, *67*(17–18), 1827–1836.

Mendes da Costa, A., M. O. Domingues, O. Mendes, and C. G. M. Brum (2011), Interplanetary medium condition effects in the south atlantic magnetic anomaly: A case

study, *Journal of Atmospheric and Solar-Terrestrial Physics*, *73*(11–12), 1478–1491.

Occhipinti, G., P. Lognonné, E. A. Kherani, and H. Hébert (2006), 3D Waveform modeling of ionospheric signature induced by the 2004 Sumatra tsunami. *Geophysical Research Letters*, *33*, L20104.

Occhipinti, G., A. Kherani , P. Lognonné (2008), Geomagnetic dependence of ionospheric disturbances induced by tsunamigenic internal gravity waves. *Geophysical Journal International*, *173*(3), 753–765.

Occhipinti, G., P. Dorey, T. Farges, and P. Lognonné (2010), Nostradamus: The radar that wanted to be a seismometer. *Geophysical Research Letters*, *37*(18), L18104.

Occhipinti, G., P. Coisson, J. J. Makela, S. Allgeyer, A. Kherani, H. Hébert, and P. Lognonné (2011), Three-dimensional numerical modeling of tsunami-related internal gravity waves in the Hawaiian atmosphere. *Earth Planets Space*, *63*(7), 847–851.

Occhipinti, G., L. Rolland, P. Lognonné, S. Watada (2013), From Sumatra 2004 to Tohoku-Oki 2011: The systematic GPS detection of the ionospheric signature induced by tsunamigenic earthquakes. *Journal of Geophysical Research: Space Physics*, *118*(6), 3626–3636.

Rolland, L., G. Occhipinti, P. Lognonné, and A. Loevenbruck (2010), Ionospheric gravity waves detected offshore Hawaii after tsunamis. *Geophysical Research Letters*, *37*(17), L17101.

Rolland, L., P. Lognonné, and H. Munekane (2011), Detection and modeling of Rayleigh wave induced patterns in the ionosphere. *Geophysical Research Letters*, *116*, A05320.

Sladen, A., H. Hébert, F. Schindelé, and D. Reymond (2007), Evaluation of far-field tsunami hazard in French Polynesia based on historical data and numerical simulations.

Natural Hazards and Earth System Science, *7* (2), 195–206.

Sladen, A., H. Hébert (2008), On the use of satellite altimetry to infer the earthquake rupture characteristics: application to the 2004 Sumatra event. *Geophysical Journal International*, *172* (2), 707–714.

Utada, H., H. Shimizu, T. Ogawa, T. Maeda, T. Furumura, T. Yamamoto, N. Yamazaki, Y. Yoshitake and S. Nagamachi (2011), Geomagnetic field changes in response to the 2011 off the Pacific Coast of Tohoku Earthquake and Tsunami, *Earth and Planetary Science Letters*, *311* (1–2), 11–27.
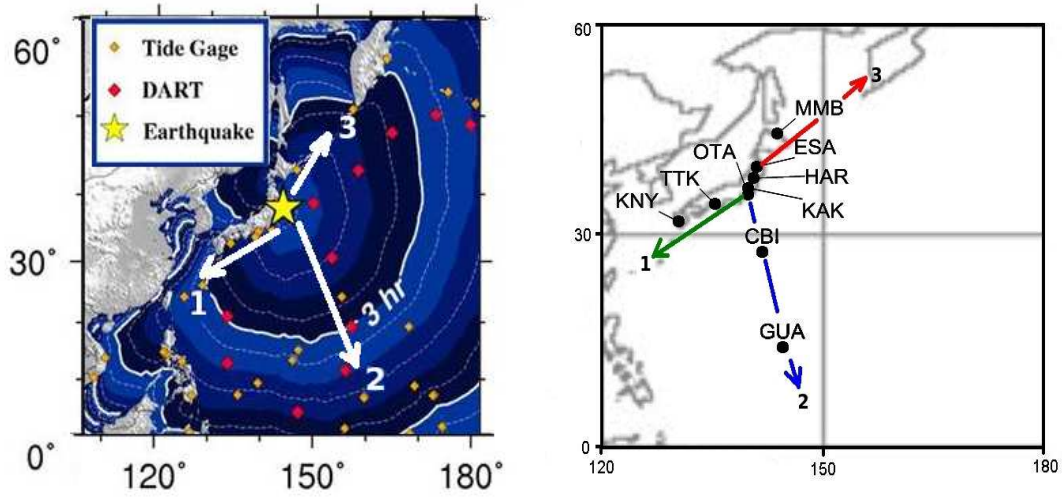
Figure 1.   TTT map and map of the geographic localization of the magnetic observatories. TTT map courtesy of NOAA/NWS/West Coast and Alaska Tsunami Warning Center.
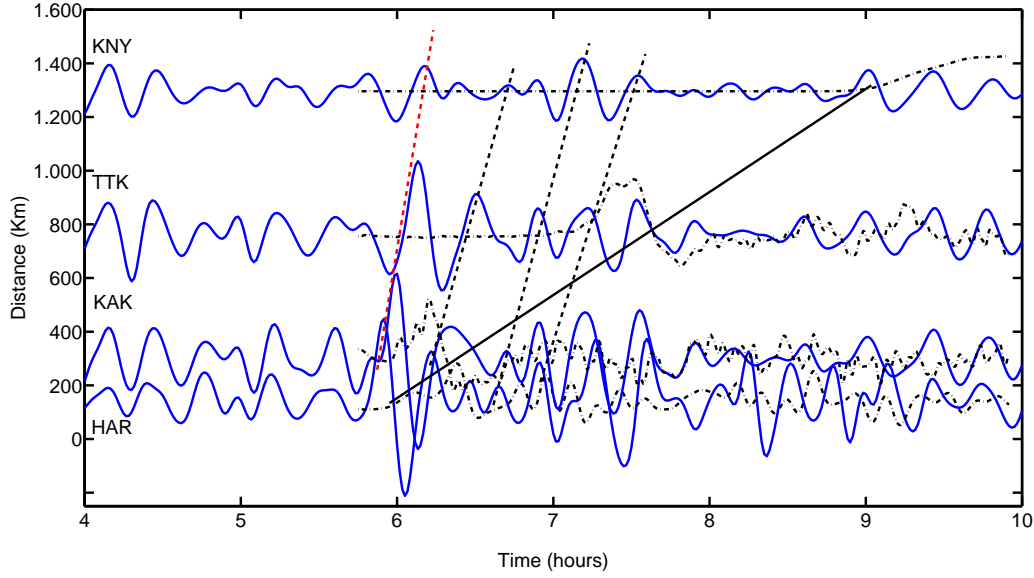
Figure 2.   Z-component dataset filtered with a bandpass with periods between 10 and 30 minutes. On the vertical axis, it is shown the distance between the earthquake epicenter and the magnetic observatory, and on the horizontal axis, the universal time. The continuous line represents the tsunami waves propagation at $\cong 200m/s$, the red dashed line is associated to Rayleigh waves with velocity of $\cong 1.3km/s$, and the black dashed lines are associated to AGWs with velocity of $\cong 640m/s$.
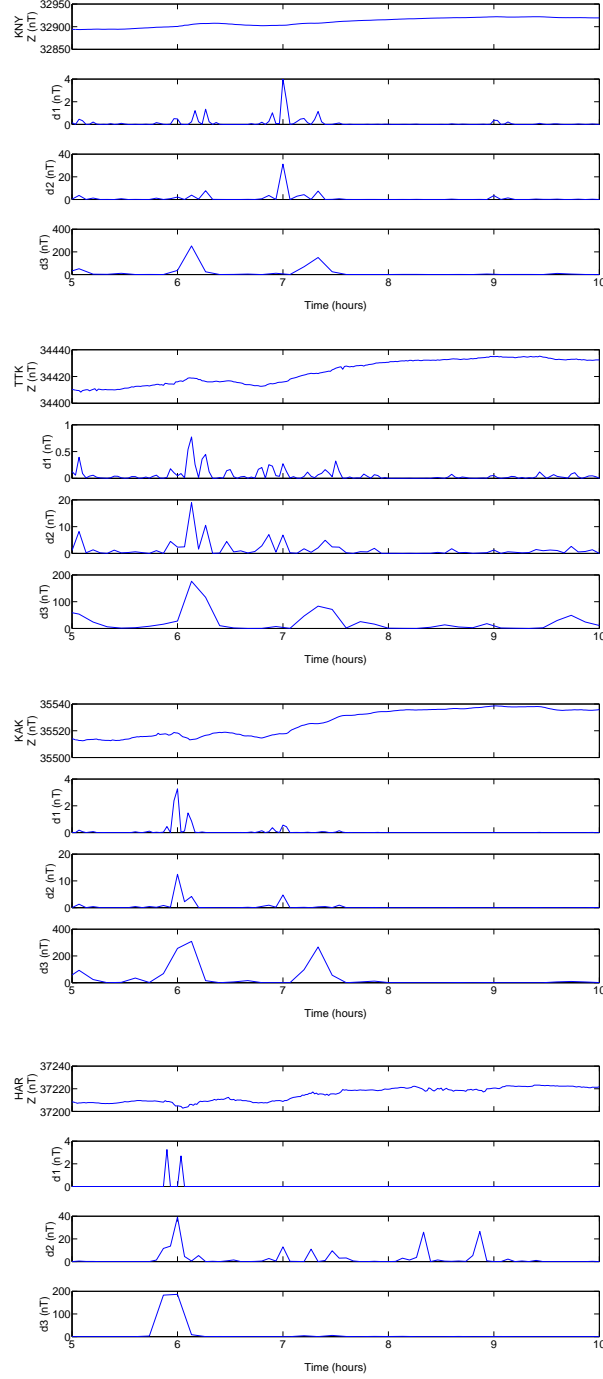
Figure 3. Magnetograms and the wavelet coefficients $(d^j)^2$ for $j = 1, 2, 3$ for wave front case study in the direction 1.
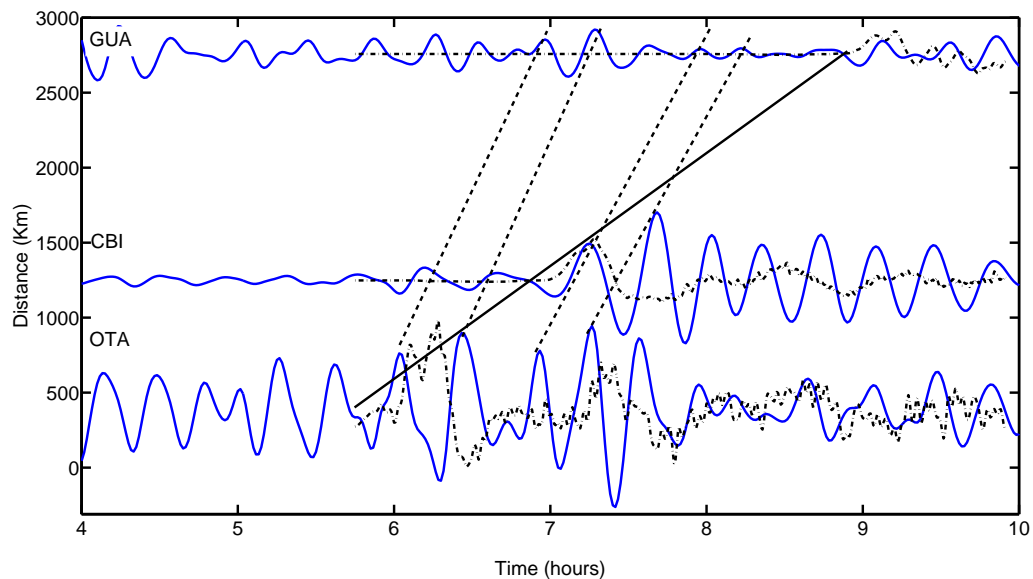
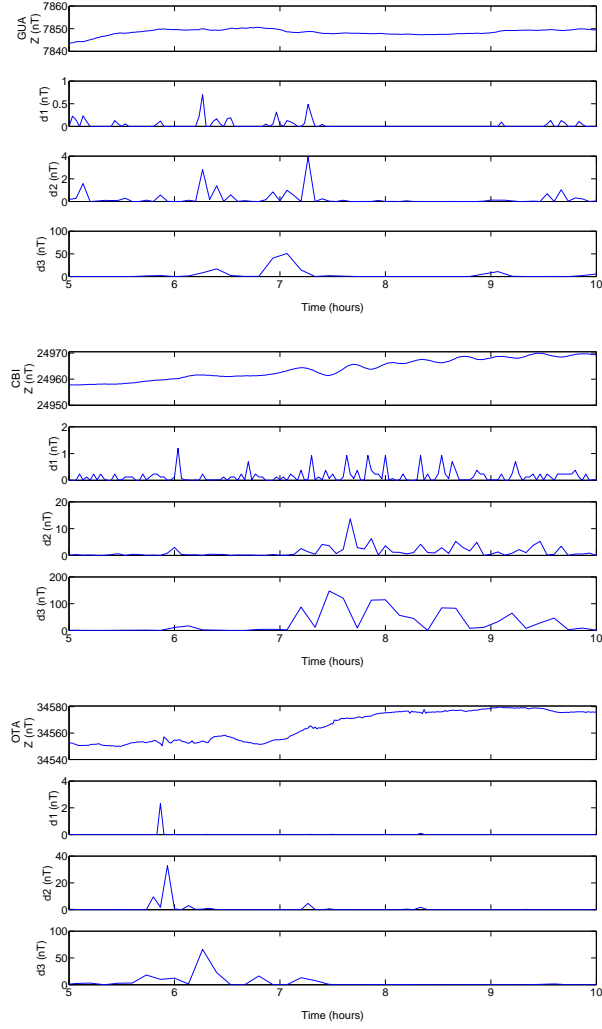**Figure 4.** Same as Fig. 1 but for the direction 2.
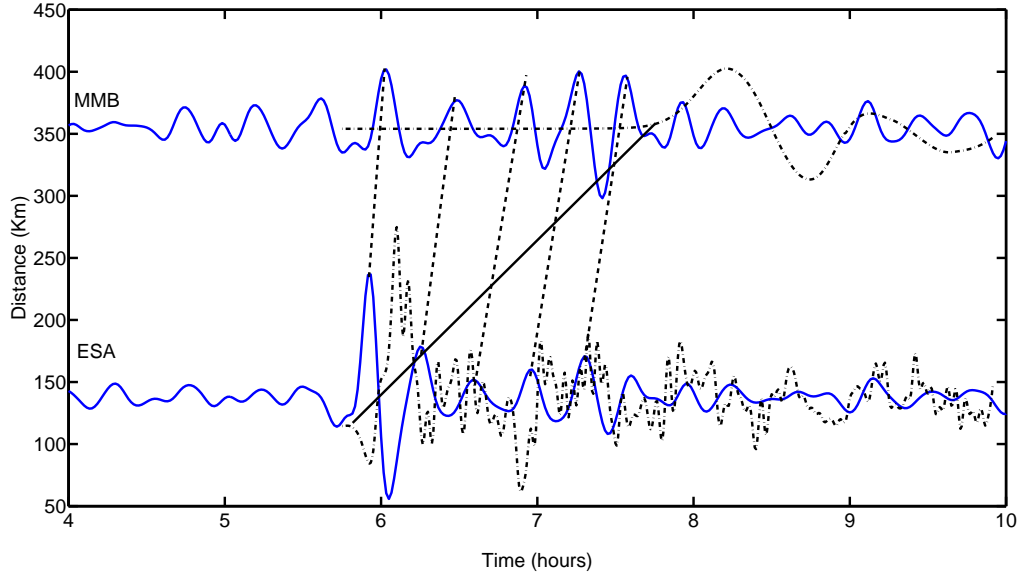
Figure 5. Same as Fig. 3 but for the direction 2.
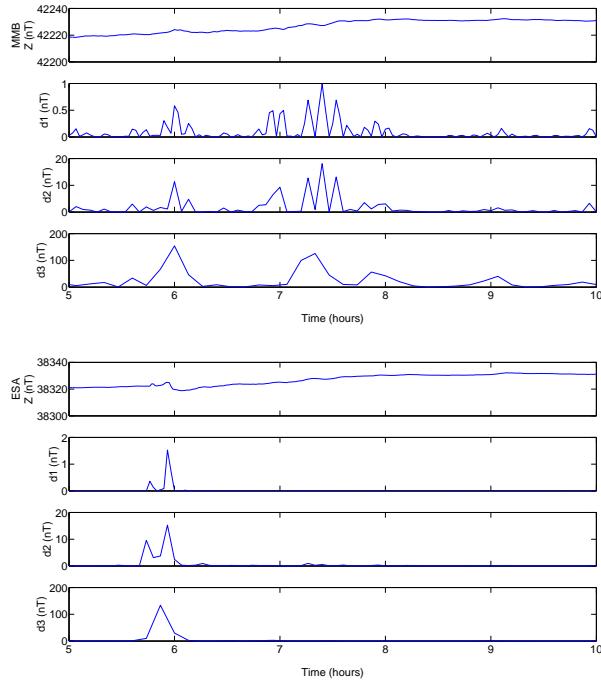
Figure 6.   Same as Fig. 1 but for the direction 3.

Figure 7.   Same as Fig. 3 but for the direction 3.

Table 1. Network of geomagnetic observatories used in this work.

IAGA code	Station	country	Geographic coord.	
			Lat.(°)	Long.(°)
CBI[1]	Chichijima	Japan	27.10	142.19
ESA[1]	Esashi	Japan	39.24	141.36
GUA	Guam	United States of America	13.59	144.87
HAR[1]	Haramachi	Japan	37.62	140.95
KAK	Kakioka	Japan	36.23	140.18
KNY	Kanoya	Japan	31.42	130.88
MMB	Memambetsu	Japan	35.44	144.19
OTA[1]	Otaki	Japan	35.29	140.23
TTK[1]	Totsugawa	Japan	33.93	135.80

[1]Observatories belonging to Geospatial Information Authority of Japan (GIS).